Journal of Power Sources 195 (2010) 5674–5685

Contents lists available at ScienceDirect

Journal of Power Sources

journal homepage: www.elsevier.com/locate/jpowsour

Integration of a molten carbonate fuel cell with a direct exhaust absorption chiller

Pere Margalef, Scott Samuelsen*

National Fuel Cell Research Center (NFCRC), University of California, Irvine, CA 92697-3550, USA

ARTICLE INFO

Article history:
Received 3 December 2009
Received in revised form 12 March 2010
Accepted 15 March 2010
Available online 19 March 2010

Keywords:
Molten carbonate fuel cell
Absorption chiller
Steady-state model
CCHP
Distributed generation

ABSTRACT

A high market value exists for an integrated high-temperature fuel cell-absorption chiller product throughout the world. While high-temperature, molten carbonate fuel cells are being commercially deployed with combined heat and power (CHP) and absorption chillers are being commercially deployed with heat engines, the energy efficiency and environmental attributes of an integrated high-temperature fuel cell-absorption chiller product are singularly attractive for the emerging distributed generation (DG) combined cooling, heating, and power (CCHP) market. This study addresses the potential of cooling production by recovering and porting the thermal energy from the exhaust gas of a high-temperature fuel cell (HTFC) to a thermally activated absorption chiller. To assess the practical opportunity of serving an early DG-CCHP market, a commercially available direct fired double-effect absorption chiller is selected that closely matches the exhaust flow and temperature of a commercially available HTFC. Both components are individually modeled, and the models are then coupled to evaluate the potential of a DG-CCHP system. Simulation results show that a commercial molten carbonate fuel cell generating 300 kW of electricity can be effectively coupled with a commercial 40 refrigeration ton (RT) absorption chiller. While the match between the two "off the shelf" units is close and the simulation results are encouraging, the match is not ideal. In particular, the fuel cell exhaust gas temperature is higher than the inlet temperature specified for the chiller and the exhaust flow rate is not sufficient to achieve the potential heat recovery within the chiller heat exchanger. To address these challenges, the study evaluates two strategies: (1) blending the fuel cell exhaust gas with ambient air, and (2) mixing the fuel cell exhaust gases with a fraction of the chiller exhaust gas. Both cases are shown to be viable and result in a temperature drop and flow rate increase of the gases before the chiller inlet. The results show that no risk of cold end corrosion within the chiller heat exchanger exists. In addition, crystallization is not an issue during system operation. Accounting for the electricity and the cooling produced and disregarding the remaining thermal energy, the second strategy is preferred and yields an overall estimated efficiency of 71.7%.

1. Introduction

The depletion and limited availability of natural resources are driving the development and deployment of more efficient power generation and electrical distribution patterns. Distributed generation (DG) is one example where small-scale power generation (<50 MW) is located close to the load being served. Transmission losses are avoided and heat which would otherwise be exhausted can be captured and used and thereby (1) achieve overall efficiencies in excess of 70%, (2) reduce proportionally the emission of greenhouse gases (GHGs), and (3) mitigate the emission of criteria pollutants. The recovery and use of heat in DG applications, regularly referred to as combined heat and power (CHP), is today increasing in popularity throughout the world.

One of the main challenges in the design of DG-CHP systems is the effective utilization of heat. Today, it is common to use the heat to augment space heating and the heating of hot water in buildings, and to produce steam in industrial applications. In many cases, especially in warm climates, the use of the thermal energy to meet cooling loads is more compelling. Absorption chillers can meet this demand and shift cooling from an electric load to a thermal load. The shift can be particularly cost-effective for facilities with time-of-day electrical rates or high cooling season rates [1]. The net result is a distributed generation combined cooling, heating, and power (DG-CCHP) system.

While absorption chillers have been regularly combined with heat engines, this paradigm has not yet been captured by the stationary fuel cell market. The market is understandably focused on the relatively less complex DG-CHP applications. The maturation of this market is now at the point where attention can now include the burgeoning DG-CCHP opportunity.

As an initial step, this study addresses the readiness, applicability, utility, and suitability of commercially available fuel cell and absorption chiller products as an early DG-CCHP market entry. In particular, a commercially available molten carbonate fuel cell and commercially available absorption chiller are evaluated for

* Corresponding author. Tel.: +1 949 824 5468; fax: +1 949 824 7423.
E-mail address: gss@apep.uci.edu (S. Samuelsen).

0378-7753/$ – see front matter © 2010 Elsevier B.V. All rights reserved.
doi:10.1016/j.jpowsour.2010.03.051

Nomenclature

AC	absorption chiller
C_p	specific heat
CCHP	combined cooling, heating and power
CHP	combined heat and power
COP	coefficient of performance
DC	direct current
DFC	direct fuel cell
DG	distributed generation
EES	engineering equation solver
FCE	FuelCell Energy, Inc
GHG	green house gas
h	convection heat transfer coefficient
HTFC	high-temperature fuel cell
LHV	lower heating value
LiBr	lithium bromide
MCFC	molten carbonate fuel cell
MTG	gas microturbine
P	pressure
P_v	vapor pressure
Q	thermal energy
RT	tones of refrigeration
S/C	steam-to-carbon ratio
SOFC	solid oxide fuel cell
T	temperature
x	LiBr concentration [%wt]
$\dot{m}$	mass flow rate
x_{shift}	percentage of CO shifted to CO_2

Subscripts

ADP	acid dew point
ch	cooling
ch_exh	chiller exhaust
exh	exhaust gas
fc_exh	fuel cell exhaust
i	point i
gen	generated product
an	anode
ca	cathode
ox	catalytic burner
smr	steam methane reforming
wgs	water–gas shift
g1	primary generator
g2	secondary generator

the production of 300 kW of steady and reliable electrical power and 40 refrigeration tons (RT) of cooling in support of a generic but realistic commercial building. To conduct the evaluation, models for both the fuel cell and absorption chiller are developed, integrated, and then applied to characterize the performance of the DG-CCHP system. The net result is to determine whether and how commercially available products can be combined to produce a viable fuel cell based DG-CCHP system for deployment into an emerging, fertile market.

2. Fuel cell system

The fuel cell adopted for this study is based on the DFC300MA® molten carbonate fuel cell (MCFC) manufactured by FuelCell Energy (FCE). This commercial unit has led the early high-temperature stationary fuel cell (HTFC) market and is well matched to the electrical and thermal requirements of commercial office buildings. Over 20 MW of MCFC is deployed in California today, all in DG-CHP applications but none in DG-CCHP applications. To assess the available thermal energy from the fuel cell that can be used for cogeneration in the absorption chiller, the exhaust gas composition, temperature and heat capacity must be established as a function of the air, fuel and water inputs into the system and utilization factors in the stack. A fuel cell model provides the vehicle for establishing this information.

Table 1
Fuel cell input parameters based on DFC300MA®.

Parameter	Value	Units	Comments
Power output	0.3	MW	ISO conditions.
Electrical efficiency	47	%	LHV based
Fuel input	0.018	$\frac{m^3(N)}{s}$	Natural gas $\left(\text{LHV} = 34\frac{MJ}{m^3}\right)$
Water input	0.150	$\frac{l}{s}$	On average
Water used	0.063	$\frac{l}{s}$	Rest rejected during the purification

2.1. Fuel cell model

The fuel cell system is modeled assuming steady-state, baseload operation. The software Engineering Equation Solver (EES), which is designed for steady-state modeling with built-in mathematical and thermo-physical property functions of working fluids, is used for the engineering calculations.

The fuel cell model takes into account the reactions that take place within the anode, cathode, electrolyte and catalytic burner. The electrochemistry of the system is not evaluated from the thermodynamic side but rather from a thermal mass balance approach. Nernst voltage, polarization losses are not evaluated. Rather, a nominal power generation and electrical efficiency level are assumed. A mass-thermal balance of the fuel cell is performed to establish the composition and specific heat of the exhaust gases. In order to predict the exhaust gas temperature, an energy balance is considered which takes into account the required heat to preheat the fuel–vapor mixture up to the pre-reformation temperature and up to the operating temperature. Table 1 shows the required fuel and water inputs required to produce 300 kW of electric power at 47% electrical efficiency [2].

2.2. Model assumptions

The assumptions for the model include:

- Operation: steady-state
- Natural gas fuel: 100% methane;
- Steam-to-carbon ratio: 3;
- Stack operating temperature: 650 °C;
- Operating system pressure: 1.2 bar;
- Steam reforming and water–gas shift reaction: occur very fast and simultaneously;
- Steam methane reforming reaction: $CH_4 + H_2O \rightarrow CO + 3H_2$
- Water–gas shift reaction: $CO + H_2O \rightarrow CO_2 + H_2$
- In the anode, not all the CO is shifted to CO_2 since; at the operating temperatures; the equilibrium point for the water–gas shift reaction is well to the left of the water–gas shift reaction [3].
- At the operating temperatures, the steam reformation and water–gas shift reaction product gas is a mix of hydrogen, carbon monoxide, carbon dioxide, and unreacted steam and methane [3];
- The remaining carbon monoxide and methane is electrolyzed within the anode compartment;
- Utilization factors for hydrogen, carbon monoxide and methane within the stack are 75% [4];

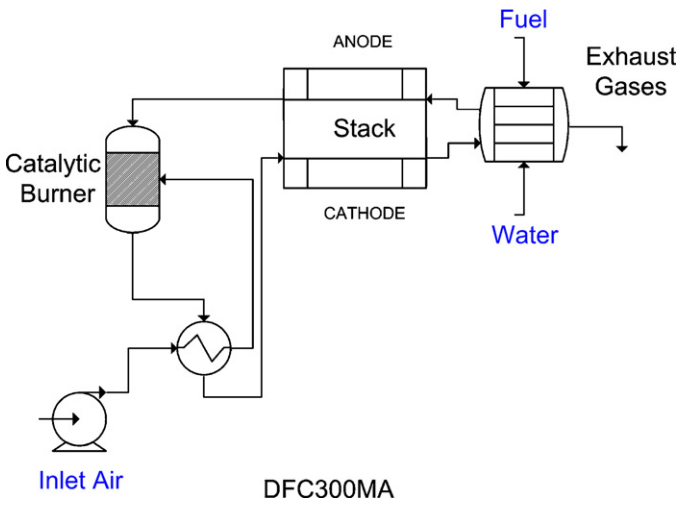

Fig. 1. DFC300MA model schematics.

2.3. Reactions and equations

Fig. 1 shows the schematic for the DFC300MA® system. The anodic gases are oxidized in the catalytic burner and recirculated to the cathode compartment. Fuel and water are preheated in the Heat Recovery Unit (HRU) before entering the stack. For each component of the fuel cell system, reactions and equations are specified.

2.3.1. Steam methane reformation (SMR) and water-shift reaction (WSR)

The steam methane reformation (SMR) and water-shift reaction (WSR) are the first processes to specify for the fuel cell model. The reaction chemistry and mass balance equations selected to characterize these processes are as follows:

- SMR reaction:

$$CH_4 + H_2O \rightarrow +3H_2 + CO$$

- SMR mass balance equations:

$$\dot{n}_{CH_4} = \dot{n}_{CH_4,in} \cdot u_{f\_CH_4}$$

$$\dot{n}_{H_2,smr} = 3 \cdot \dot{n}_{CH_4,in}$$

$$\dot{n}_{CO,smr} = \dot{n}_{CH_4,in}$$

- WSR reaction:

$$CO + H_2O \rightarrow CO_2 + H_2$$

- WSR mass balance equations:

$$\dot{n}_{H_2,wsr} = \dot{n}_{CO,smr} \cdot x_{shift}$$

$$\dot{n}_{CO_2,wsr} = \dot{n}_{CO,smr} \cdot x_{shift}$$

2.3.2. Anode reactions

After reformation and the water–gas shift reaction, the hydrogen and carbon monoxide products combine with carbonate ions to produce water, carbon dioxide and electrons within the anode compartment. Carbon dioxide is recirculated to the cathode compartment in order to complete the cathode reactions.

- Reactions:

$$H_2 + CO_3^{=} \rightarrow H_2O + CO_2 + 2e^-$$

$$CO + CO_3^{=} \rightarrow 2CO_2 + 2e^-$$

- Mass balance equations:

$$\dot{n}_{H_2,an} = \dot{n}_{H_2,smr} + \dot{n}_{H_2,wsr}$$

$$\dot{n}_{CO,an} = \dot{n}_{CO,smr} \cdot (1 - x_{shift})$$

$$\dot{n}_{H_2O,an} = \dot{n}_{H_2O,in} - \dot{n}_{CH_4} - \dot{n}_{CO,smr} \cdot x_{shift}$$

$$\dot{n}_{H_2O,gen,an} = \dot{n}_{H_2,an}$$

$$\dot{n}_{CO_2,gen,H_2} = \dot{n}_{H_2,an}$$

$$\dot{n}_{CO_2,gen,CO} = 2 \cdot \dot{n}_{CO,an}$$

2.3.3. Anode exhaust

The utilization factor of the fuel species x (u_{f-x}) determines how much of the fuel species x is used within the stack to produce electricity. The rest of the fuel is oxidized in the catalytic oxidizer and its thermal energy is used in the fuel cell balance of plant to preheat the air, water and fuel streams. The remaining thermal energy is available for cogeneration.

At the anode exhaust, the molar flow rates of each species are estimated by the following equations:

$$\dot{n}_{H_2,an,exh} = \dot{n}_{H_2,an} \cdot (1 - u_{f\_H_2})$$

$$\dot{n}_{CO,an,exh} = \dot{n}_{CO,an} \cdot (1 - u_{f\_CO})$$

$$\dot{n}_{CH_4,an,exh} = \dot{n}_{CH_4,in} \cdot (1 - u_{f\_CH_4})$$

and, during the fuel cell reactions, water and carbon dioxide are generated as follows:

$$\dot{n}_{CO_2,an,exh} = \dot{n}_{CO_2,wsr} + \dot{n}_{CO_2,gen,H_2} + \dot{n}_{CO_2,gen,CO}$$

$$\dot{n}_{H_2O,an,exh} = \dot{n}_{H_2O,an} + \dot{n}_{H_2O,gen,an}$$

2.3.4. Catalytic oxidizer

Unused fuel (consisting of hydrogen, carbon monoxide and methane) is oxidized in the catalytic oxidizer in order to produce heat, carbon dioxide and water. The carbon dioxide produced is used in the cathode. The first step is to determine the stoichiometric or theoretical air of the catalytic reaction (based on "complete combustion reaction" where only the major products of CO_2, H_2O, and N_2 are considered):

- Reaction (complete combustion):

$$AH_2 + BCO + CCH_4 + a(O_2 + 3.76N_2) \rightarrow bCO_2 + cH_2O + dN_2$$

where a is the stoichiometric number of moles of O_2. The actual reaction is

- Reaction (actual):

$$AH_2 + BCO + CCH_4 + a \cdot Y \cdot (O_2 + 3.76N_2) \rightarrow b'CO_2 + c'H_2O + d'N_2 + eO_2$$

where the parameter Y represents the deviation from stoichiometric. The gas leaving the oxidizer is transported to the cathode compartment where the cathode reactions take place.

2.3.5. Cathode reactions

The oxygen and the carbon dioxide present in the catalytic combustor exhaust gas combine with the electrons (i.e., reduction) to form the carbonate ion that will travel to the anode compartment through the electrolyte:

- Reaction:

$$\frac{1}{2}O_2 + CO_2 + 2e^- \rightarrow CO_3^=$$

- Mass balance equations:

$$\dot{n}_{CO_2,ca,in} = \dot{n}_{CO_2,a,,exh} + \dot{n}_{CO_2,ox,exh}$$

$$\dot{n}_{H_2O,ca,in} = \dot{n}_{H_2O,an,exh} + \dot{n}_{H_2O,ox,exh}$$

$$\dot{n}_{O_2,ca,in} = \dot{n}_{O_2,ox,exh}$$

$$\dot{n}_{N_2,ca,in} = \dot{n}_{N_2,ox,exh}$$

$$\dot{n}_{CO_3,prod} = \dot{n}_{H_2,an,ox} + \dot{n}_{CO,an,ox}$$

$$\dot{n}_{O_2,used,ca} = 0.5 \cdot \dot{n}_{CO_3,prod}$$

$$u_f = \frac{\dot{n}_{O_2,used,ca}}{\dot{n}_{O_2,ca,in}}$$

$$\dot{n}_{CO_2,cons,ca} = \dot{n}_{CO_3,prod}$$

2.3.6. Stack exhaust

The final products are determined using the following equations:

- Mass balance equations:

$$\dot{n}_{CO_2,ca,exh} = \dot{n}_{CO_2,ca,in} - \dot{n}_{CO_2,cons,ca}$$

$$\dot{n}_{H_2O,ca,exh} = \dot{n}_{H_2O,ca,in}$$

$$\dot{n}_{O_2,ca,exh} = \dot{n}_{O_2,ca,in} - \dot{n}_{O_2,cons,ca}$$

$$\dot{n}_{N_2,ca,exh} = \dot{n}_{N_2,ca,in}$$

where the total molar flow rate of the fuel cell exhaust gas is:

$$\dot{n}_{exh} = \dot{n}_{CO_2,ca,exh} + \dot{n}_{H_2O,ca,exh} + \dot{n}_{O_2,ca,exh} + \dot{n}_{N_2,ca,exh}$$

and the mass flow rate $\dot{m}_{exh}$ is obtained by multiplying the molar flow rate with the corresponding molar weight of each species.

2.3.7. Energy balance

To predict the absorption chiller behavior, it is necessary to determine the fuel cell exhaust gas temperature. To accomplish this step, the following assumptions are made:

- The reforming reactions (endothermic) occur within the anode and are heated by the thermal energy released during the fuel cell reactions (exothermic).
- The fuel–water vapor mixture is first pre-reformed and then heated up to 650 °C (fuel cell stack temperature) utilizing exhaust gas heat.
- The inlet air is preheated with the exhaust gas before entering the catalytic oxidizer.
- Heat losses induced by free convection heat flux are estimated by:

$$losses_{conv} = A \cdot h \cdot (T_s - T_\infty)$$

Where A (m^2) is the vertical surface of the stack, h is the convection heat transfer coefficient ($W\,m^{-2}\,K^{-1}$) and T_S and T_∞ are the temperatures at the surface and of the environment, respectively. The value used for h was $0.025\,W\,m^{-2}\,K^{-1}$ (P. Incropera, 2001).

The total energy balance equation is:

- Energy balance equation:

$$\dot{m}_{exh}c_{p_{exh}}(T_{stack} - T_{exh}) = loss_{conv} + \dot{m}_{CH_{4,in}}c_{p_{CH_4}}(T_{preref,in} - T_{amb}) + (\dot{m}_{CH_{4,in}} + \dot{m}_{H_2O})c_{p_{preref}}(T_{stack} - T_{preref,out}) + \dot{m}_{exh}c_{p_{air}}(T_{preheat} - T_{amb})$$

Table 2 summarizes the results obtained from the fuel cell model simulations. As seen, the specific heat, mass flow rate and temperature of the fuel cell exhaust gas can be established as a function of the cathode excess air. These results have been validated with data from the fuel cell manufacturer [2].

3. Absorption chiller system

The selection of the absorption chiller must be based on an attractive match to the effluent temperature and exhaust flow rate of the DFC300MA®. The commercially available 40RT Yazaki CH4040-KE fortuitously meets this requirement. The chiller is a dual exhaust and gas fired double-effect chiller which (1) takes exhaust gases directly as the heat source and is supported by a high-temperature generator (HGE) which burns natural gas in case of insufficient thermal energy, and (2) uses lithium bromide-water ($LiBr–H_2O$) solution as a working fluid, water as a refrigerant, and $LiBr–H_2O$ as the absorbent [5,6].

Fig. 2 represents the schematic of the Yazaki CH4040-KE system. Dilute LiBr solution in the primary generator (EGE) is heated and boiled as a result of the flow of the fuel cell hot gases (Q_{IN}). As the solution boils, refrigerant vapor (steam) separates from solution and flows down into the secondary generator (LGE) coil. The $LiBr–H_2O$ solution, thereby increased in concentration (semi-concentrated state), continues upwards filling the heat pump tube and flowing down to the high-temperature heat exchanger (HHE)

Table 2
Fuel cell simulation results.

Excess air *Y*	C_p exhaust [kJ (kg K)$^{-1}$]	Exhaust mass flow rate [lb h^{-1}]	Exhaust mass flow rate [kg s^{-1}]	Exhaust Temp [C]
4.5	1.251	3947	0.4973	353.6

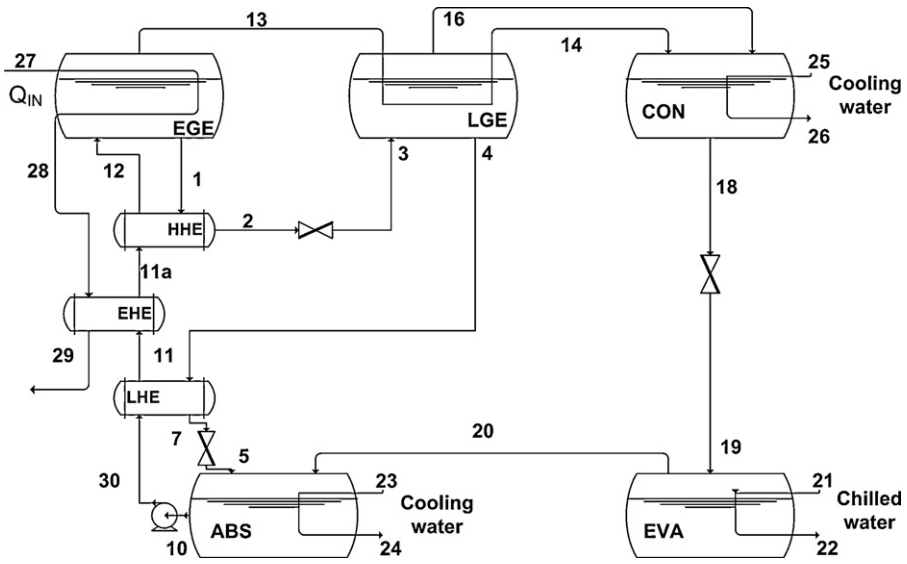

Fig. 2. Double-effect absorption chiller model schematics.

before arriving at the LGE chamber for the secondary boiling process. The HHE transfers heat from the semi-concentrate to the dilute solution.

The condensed refrigerant in the LGE coil, and the separated refrigerant vapor in the LGE chamber, enter the condenser (CON) where condensation is completed before entering to the evaporator (EVA). Heat of condensation in the CON is transferred to the cooling water and rejected at the cooling tower.

The concentrated $LiBr–H_2O$ solution produced in the LGE passes through the low temperature heat exchanger (LHE) transferring its heat to the dilute LiBr solution before entering the absorber (ABS). The $LiBr–H_2O$ solution concentration and temperature of the cooling water provides the low pressure environment under which the liquid refrigerant changes phase over the EVA coil. As the LiBr solution in the ABS absorbs the refrigerant vapor, produced in the EVA, dilute solution is once again formed. Heat of absorption is transferred to the cooling water flowing from the cooling tower [6].

Table 3 shows the rated COP and cooling capacity at nominal conditions.

3.1. Absorption chiller model

The CH4040-KE unit is designed to be coupled with heat engines, the exhaust gas streams of which differ significantly in composition, temperature and pressure from that of the molten carbonate fuel cell exhaust gas stream. As a result, it is necessary to establish the behavior of the chiller as a function of the inlet stream.

Table 3
Yazaki performance at nominal conditions.

	Nominal point	Units
Inlet temperature	280	°C
Inlet flow rate	0.78	kg s^{-1}
COP	1.06	
Cooling capacity (Q_{CH})	141	kW

To accomplish this, a chiller model was developed to establish the concentration, temperature, and pressure at every point of the system as well as the generated cooling and coefficient of performance (COP) as a function of the inlet stream (i.e., the fuel cell exhaust gas). The software Engineering Equation Solver (EES) was adopted for the calculations using libraries based on the ASHRAE Fundamentals Handbook [7].

3.2. Model assumptions

For the model, the following assumptions were made:

- Operation: steady-state
- Chilled water and cooling water input temperatures: constant;
- The concentration of the diluted solution (Stream 12): constant. Note, the diluted solution mass flow rate (Streams 30, 11, 11a, 12), driven by the solution pump from the absorber bottom to the exhaust gas generator (EGE), is constant
- The solution pump (SP): adiabatic. Therefore $h_{10} = h_{30}$;
- High level pressure (P_{high}) is assumed constant whereas medium (P_{med}) and low (P_{low}) pressures are defined as a function of the condenser and evaporator temperatures, respectively. High pressure level is a function of the temperature of the solution leaving the LGE (T_4). However, because of software limitations, when high pressure is so defined, the model does not converge. Thus, higher pressure level is assumed constant at P_{high} = 86.65 kPa, which is the value at the nominal operation point. Since T_4 remains reasonably constant when changing the input parameters, the error associated to this assumption can be neglected;
- The state of the refrigerant at point 14: saturated liquid. Therefore, from point 13 (superheated vapor) to point 14, all the vaporization heat plus some sensible heat is used to extract extra refrigerant from the solution;
- The state of the refrigerant at point 20: saturated vapor. Therefore, all refrigerant is being vaporized within the evaporator by absorbing heat from the chilled water [8].

- No pressure losses between the evaporator and the absorber are considered;
- Throttling devices are assumed isenthalpic;
- The HGE is not incorporated with the goal to operate the chiller, if possible, without consuming additional fuel and emitting corresponding criteria pollutants.

3.3. Equations

3.3.1. Primary generator (EGE)

The exhaust flow from the fuel cell heats and vaporizes the refrigerant vapor within the primary generator (EGE). The energy balance between the exhaust heat gas and the *LiBr–H_2O* solution are described by the following equations [9]:

$$Q_{g1} = \dot{m}_{exh} \cdot Cp_{exh} \cdot (T_{27} - T_{28})$$

$$Q_{g1} = \dot{m}_{13}h_{13} + q_{g1} + \dot{m}_1 h_1 - \dot{m}_{12}h_{12}$$

where q_{g1} represents the free convection heat losses:

$$q_{g1} = A_{g1}h(T_s - T_\infty)$$

and A_{g1} is the vertical surface of the first generator, h is the convection heat transfer coefficient, T_s is the temperature at the generator surface and T_∞ is the ambient temperature [10]. To satisfy mass conservation,

$$\dot{m}_{13} = \dot{m}_{12} - \dot{m}_1$$

$$\dot{m}_{13} = \dot{m}_{12}(1 - x_{12}) - \dot{m}_1(1 - x_1)$$

where $\dot{m}_i$ and x_i are the mass flow rate and the LiBr mass concentration at point i. Through lithium bromide EES libraries, the solution temperature as a function of pressure and concentration can be determined.

$$T_1 = f(LiBr, P_{high}, x_1)$$

(Note: The previous equation corresponds to the EES' expression to call the temperature at equilibrium of lithium bromide-water solution of concentration x_1 (LiBr wt.%) at pressure P_{high}.)

Enthalpy at point 13 can be determined since steam leaves the generator at P_{high}. Temperature within the generator is higher than the saturation temperature at the operating pressure. Therefore, the steam produced is superheated.

$$h_{13} = f(Superheated\_steam, P_{high}, T_1)$$

(Note: The LiBr libraries can be used only at equilibrium. For instance, temperature at point 12 cannot be determined by the libraries since at this point it has been affected by the heat exchangers [11].)

3.3.2. Secondary generator (LGE)

The pressure at the secondary generator is a function of the temperature at the condenser ($T_{condenser}$). To enhance the heat transfer between the cooling water and the refrigerant, the operating temperature within the condenser has to be 3–4° higher than the cooling water [5].

$$P_{med} = P_{sat}(water, T_{condenser})$$

Refrigerant vapor from the primary generator will extract more refrigerant from the solution within the secondary generator. The energy balance equations are:

$$Q_{g_2} = \dot{m}_{14}(h_{13} - h_{14})$$

$$Q_{g_2} = \dot{m}_{16}h_{16} + q_{g2} + \dot{m}_3 h_3 - \dot{m}_4 h_4$$

where q_{g2} are free convection heat losses:

$$q_{g2} = A_{g2}h(T_s - T_\infty)$$

To satisfy the mass conservation,

$$\dot{m}_3 = \dot{m}_{16} + \dot{m}_4$$

$$\dot{m}_{16} = \dot{m}_3(1 - x_3) - \dot{m}_4(1 - x_4)$$

Point 4 can be determined using LiBr library since it assumed to be at equilibrium. Thus,

$$T_3 = f(LiBr, P_{med}, x_3)$$

$$h_3 = f(LiBr, T_3, x_3)$$

$$T_4 = f(LiBr, P_{med}, x_4)$$

$$h_4 = f(LiBr, T_4, x_4)$$

$$h_{16} = f(Superheated\_steam, P_{med}, T_{condenser})$$

3.3.3. Condenser (CON)

In the condenser, heat of vaporization from the refrigerant vapor is rejected at the cooling tower through the cooling water circuit. Energy balance between the refrigerant side and the water cooling system are described by:

$$Q_{con} = \dot{m}_{cooling}Cp_{water}(T_{26} - T_{25})$$

$$Q_{con} = \dot{m}_{18}(h_{16} - h_{18})$$

where:

$$h_{18} = f(water, P_{med}, T_{18})$$

$$T_{18} = T_{sat}(water, P_{med})$$

To satisfy mass conservation,

$$\dot{m}_{18} = \dot{m}_{14} + \dot{m}_{16}$$

Saturated liquid is throttled by valve 19. Since it is an isenthalpic valve,

$$h_{18} = h_{19}$$

Because the pressure at point 19 is lower than at point 18, the saturated liquid will turn into a vapor–liquid mixture. With pressure at point 19 (P_{low}), determined by the chilled water inlet temperature, the quality of this water–vapor mixture can be determined.

3.3.4. Evaporator (EVA)

The evaporator operates at a very low pressure, defined as:

$$P_{low} = P_{sat}(water, T_{eva})$$

where T_{eva}, defined as the chilled water temperature leaving the evaporator, has been set at 5 °C.

At the evaporator, water is chilled by extracting heat from the chilled water. Extracted heat vaporizes the liquid–vapor mixture coming from the condenser throttled by valve 19.

Energy and mass balances within the evaporator are described by equations [9]:

$$Q_{ch} = \dot{m}_{chilled}Cp_{water}(T_{22} - T_{21})$$

$$Q_{ch} = \dot{m}_{19}h_{evap}(1 - q_{19}) + q_{eva}$$

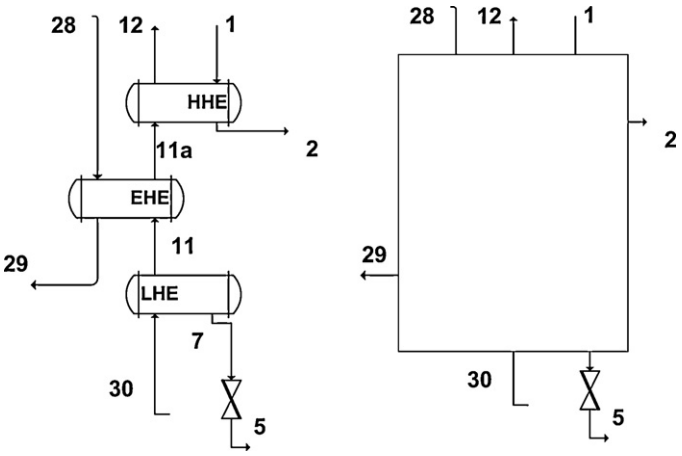

Fig. 3. Heat exchangers assumption.

$$\dot{m}_{18} = \dot{m}_{19}$$

where q_{eva} represents the free convection heat losses at the evaporator, and $(1 - q_{19})$ corresponds to the fraction of refrigerant that has not been vaporized during the isenthalpic throttling.

3.3.5. Absorber (ABS)

The pressure drop between the evaporator and absorber has been neglected since it is very small [12]. Energy balance within the absorber is described by:

$$Q_{abs} = \dot{m}_{cooling} Cp_{water}(T_{24} - T_{23})$$

$$Q_{abs} = \dot{m}_7 h_7 + \dot{m}_{20} h_{20} - \dot{m}_{10} h_{10}$$

where:

$$T_7 = f(LiBr, P_{low}, x_4)$$

$$h_7 = f(LiBr, T_7, x_4)$$

$$h_{20} = f(sat\_steam, P_{low})$$

$$T_{10} = f(LiBr, P_{low}, x_{12})$$

$$h_{10} = f(LiBr, T_{10}, x_{12})$$

Finally, to satisfy mass conservation,

$$\dot{m}_{20} = \dot{m}_{19}$$

$$\dot{m}_7 = \dot{m}_4$$

$$\dot{m}_{10} = \dot{m}_7 + \dot{m}_{20}$$

3.3.6. Heat exchangers

The three heat exchangers present in the real system (HHE, EHE and LHE) have been considered as one unique block in order to simplify the model. Fig. 3 illustrates this assumption. The energy balance equation is:

$$\dot{m}_{12}(h_{12} - h_{30}) = \dot{m}_1(h_1 - h_2) + \dot{m}_{exh}(h_{28} - h_{29}) + \dot{m}_4(h_4 - h_5)$$

where due to the isenthalpic condition of the throttling valves, it can be assumed that:

$$h_2 = h_3$$

$$h_5 = h_7$$

$$h_{30} = h_{10}$$

In order to evaluate how much heat has been extracted from the fuel cell exhaust gases and identify potential applications for remaining heat after the chiller, it is crucial to calculate h_{29} (enthalpy of the exhaust gas downstream the absorption chiller).

3.4. Efficiency evaluation

To evaluate the thermodynamic performance of the chiller itself, the coefficient of performance (COP) is estimated as follows:

$$COP = \frac{Q_{ch}}{Q_{exh} + Q_{par}}$$

where Q_{ch} is the cooling provided by the absorption chiller, Q_{exh} is the heat extracted from the fuel cell exhaust gas and Q_{par} are parasitic loads associated with the solution pumps.

4. CCHP model: fuel cell and absorption chiller integration

The fuel cell and absorption chiller models are integrated to establish a distributed generation combined cooling heating and power (DG-CCHP) system. A representation of the DG-CCHP system is illustrated in Fig. 4, where it can be appreciated how the hot fuel cell gases are directly injected into the chiller.

4.1. Critical issues

4.1.1. Cold end corrosion

One of the critical issues in matching the two systems is the potential hazard related with cold end corrosion due to acid condensation. During the combustion of any hydrocarbon, combustion products such as NO_x, SO_x, unburned hydrocarbons, PM's, soot are likely to appear. In the case of heat exchangers, these components represent a potential threat. For instance, when sulfur is oxidized, sulfur dioxide is formed and to a small extent sulfur trioxide. If the flue gas temperature drops below the acid dew temperature (T_{ADP}), the SO_3 combines with the water vapor present in the gas, forming sulfuric acid. This acid can condense on the exchanger surface materials, leading corrosion and destruction. Furthermore, if the flue gas is cooled below the water vapor dew point, CO_2 can also combine with water vapor to form carbonic acid which can attack mild steel [11]. Therefore, it is very important to calculate the sulfuric acid and water vapor dew points in order to establish a limit value for the exhaust gas temperature within the absorption chiller [12].

In the case of molten carbonate fuel cell, sulfur has to be strictly removed before entering the stack to avoid poisoning the active sites for the oxidation reduction [3]. In particular, the allowable level of hydrogen sulfide (H_2S) present in natural gas entering the fuel cell must be lower than 10 ppm. The strategy employed is to remove the sulfur from the fuel gas entering the fuel cell. As a result, it can be assumed that there is not risk of acid sulfuric formation.

Carbonic acid formation can be addressed by considering the exhaust gas as a mixture of ideal gases and thereby assume that the mole fraction, the pressure fraction, and the volume fraction of a component are identical. Therefore, from the fuel cell model results and assuming an operating pressure of $P = 1.2$ bar, the vapor pressure of the exhaust gas (P_v) is:

$$p_{v_{H_2O}} = [H_2O] = 0.2677$$

$$\frac{p_{v_{H_2O}}}{P} = 0.2677$$

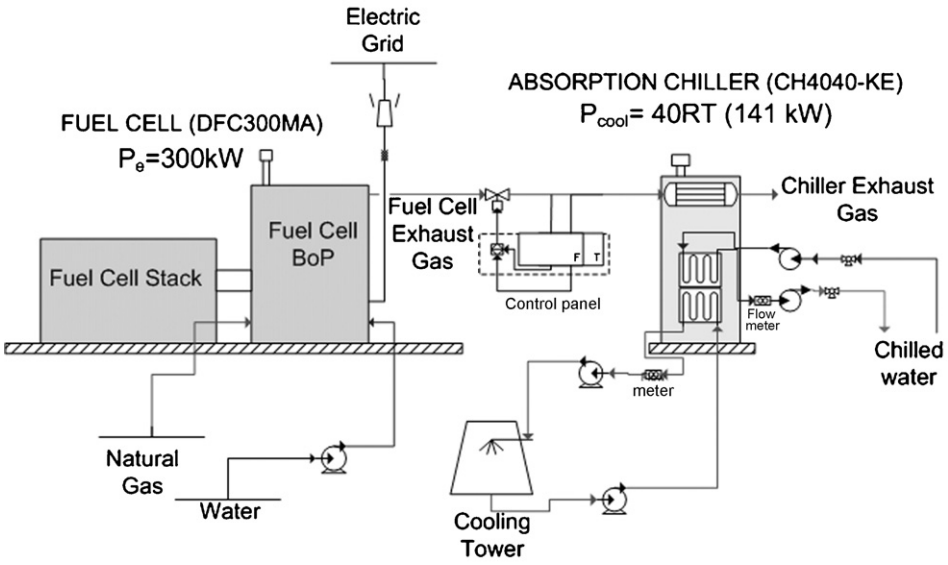

Fig. 4. HTFC-AC integrated prototype.

$p_{v_{H_2O}} = 0.32\,\text{bar} = 32.12\,\text{kPa}$

The dew-point corresponds to the saturation temperature at the vapor pressure [9]. From steam tables,

$T_{dp} = T_{sat@P_v} \approx 70\,^{\circ}\text{C}$

Since the lowest temperature within the absorption chiller is estimated to be approximately 120 °C, the risk of carbonic acid formation is negligible.

4.1.2. Crystallization nature of LiBr solution

A second critical issue is the crystallization nature of the LiBr solution. In nature, solid LiBr salt has a crystalline structure. When dissolved in water, the salt becomes an aqueous solution. However, when the mass fraction of salt exceeds the solubility limit, the salt component precipitates.

In absorption chillers, usually the crystallization line for lithium bromide and water are close to the working concentrations needed for practical $LiBr/H_2O$ absorption chillers [10]. Furthermore, crystal nucleation is a process sensitive to the presence of nucleation sites. The solubility limit is a strong function of mass fraction and temperature and a weak function of pressure. Once crystals begin to form, the crystals themselves provide favorable nucleation sites and crystals grow on themselves [5]. If the solution concentration is too high or the solution temperature is reduced too low, crystallization may occur and interrupt machine operation. Crystallization must be avoided since the formation of slush in the piping network over time could form a solid and block the flow. Once crystallization occurs, the recovery of absorber operation is labor intensive and time consuming.

4.2. Systems integration strategies

In the absence of a chiller designed to match the exhaust stream of a MCFC, a strategy is needed to optimize the performance of an installed DG-CCHP system. In this study, three different strategies were considered:

- *Strategy 0*: Chiller inlet gas is the fuel cell exhaust gas.
- *Strategy 1*: Chiller inlet gas is the fuel cell exhaust gas blended with ambient air at 25 °C.
- *Strategy 2*: Chiller inlet gas is the fuel cell exhaust gas blended with chiller exhaust at $T = T_{ch\_exh}$.

4.2.1. Strategy 0: no extra air addition

Table 4 presents the temperature and flow rate of the fuel cell exhaust gas as well as the inlet temperature and flow rate suggested by the chiller manufacturer [6]. As observed, the temperature of the fuel cell exhaust gas is higher than the chiller inlet temperature. Also, the mass flow rate of the fuel cell exhaust gases is lower than the chiller inlet flow rate. The effects of this mismatch between temperatures and flow rates will be evaluated in Strategy 0. This strategy consists of using the fuel cell exhaust gas directly as the chiller input. Fig. 5 presents the schematic for Strategy 0.

4.2.2. Strategy 1: ambient air mixing

In this strategy, fuel cell exhaust gas is blended with ambient air. Fig. 6 presents the schematic for this strategy. As seen, air at 25 °C is mixed with the fuel cell exhaust stream. The extra air flow inlet values vary from 0 to 0.4 kg s^{-1}. As a limiting value, the chiller inlet flow rate is set at 0.85 kg s^{-1}, which corresponds to the maximum amount of gas which can be introduced into the chiller primary generator (EGE).

4.2.3. Strategy 2: chiller exhaust gases injection

The chiller exhaust gases are expected to be approximately 120 °C. Strategy 2 consists on recovering part of the remaining thermal energy of the chiller exhaust gases by blending them with the fuel cell exhaust gases. The resulting gas mixture serves as the chiller input gas. Fig. 7 presents the schematic for this strategy.

Table 4
Fuel cell and chiller temperature and flow.

	Fuel cell exhaust gas	Absorption chiller
Temperature [C]	353	280
Flow rate [kg s^{-1}]	0.50	0.78

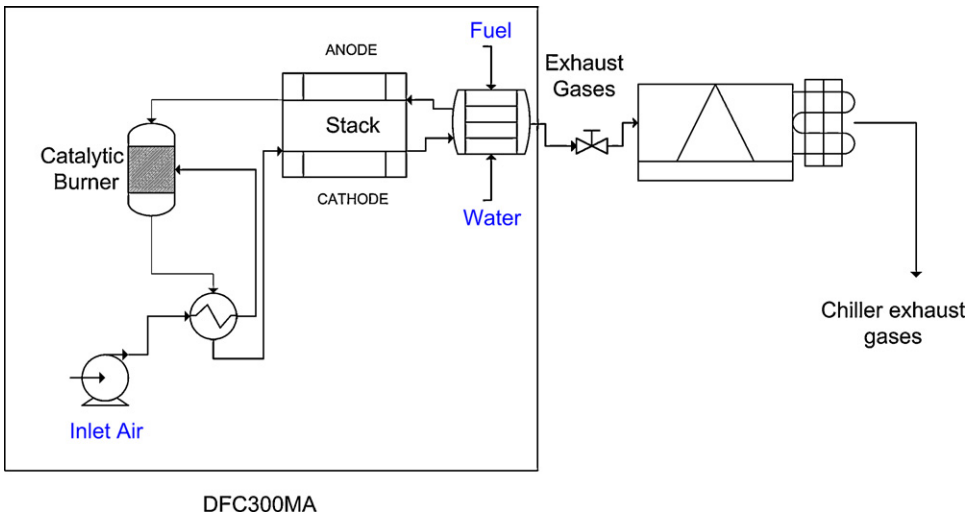

Fig. 5. Schematics of Strategy 0.

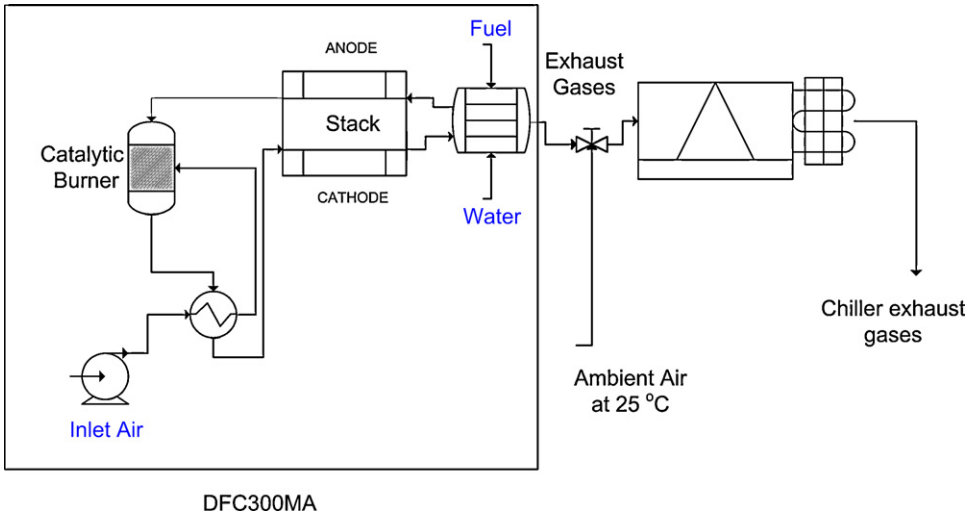

Fig. 6. Schematics of Strategy 1.

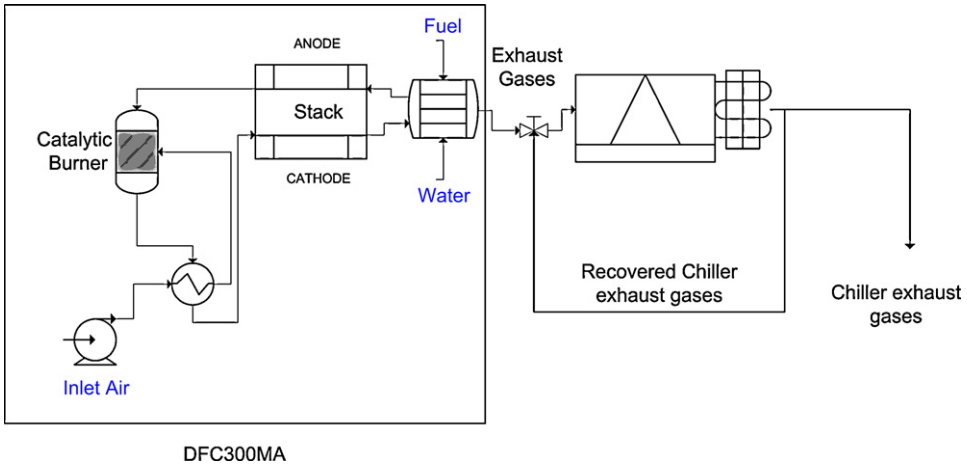

Fig. 7. Schematics of Strategy 2.

Table 5
Strategy 0 results.

m_{IN} [kg s^{-1}]	Cp_{IN} [kJ (kg K)$^{-1}$]	T_{IN} [C]	T_{OUT} [C]	Q_{IN} [kW]	Q_{CH} [kW]	COP
0.5099	1.264	336.3	137.2	128.4	131.1	1.005

Table 6
Strategy 1 performance results.

m_{FC_EXH} [kg s^{-1}]	m_{EXTRA_AIR} [kg s^{-1}]	m_{IN} [kg s^{-1}]	T_{FC_EXH} [C]	T_{IN} [C]	Cp_{FC_EXH} [kJ (kg K)$^{-1}$]	Cp_{IN} [kJ (kg K)$^{-1}$]	Q_{IN} [kW]	Q_{CH} [kW]	COP
0.5099	0	0.5099	336.3	336.3	1.264	1.264	128.4	131.1	1.005
0.5099	0.1	0.6099	336.3	294.3	1.264	1.222	117.6	121.5	1.016
0.5099	0.2	0.7099	336.3	262.3	1.264	1.191	107.1	110.9	1.017
0.5099	0.3	0.8099	336.3	237.1	1.264	1.168	96.72	99.71	1.01
0.5099	0.4	0.85	336.3	216.7	1.264	1.231	86.52	88.1	0.9952

5. Results and discussion

5.1. Strategy 0

Table 5 contains the main performance parameters of the chiller when operating with the exhaust gas as they leave the fuel cell (i.e., Strategy 0). The CCHP model takes into account the heat losses along the duct which connects the fuel cell exhaust gases to the chiller. In fact, according to the fuel cell model, the exhaust temperature was presumed to be as high as 353 °C. In this case, it drops below 340 °C when they enter the chiller.

As seen, a decrease in both the cooling capacity (Q_{ch}) and coefficient of performance (COP) occurs when compared with the nominal chiller performance (see Table 3). The biggest concern in this case is the inlet temperature. Although the model estimates the inlet temperature to be below 340 °C, FuelCell Energy states that the exhaust temperature is 370 ± 25 °C due to some heat losses reductions within the fuel cell balance of plant [2]. Such high-temperatures may induce crystallization issues in the chiller absorber where LiBr solution concentration is at its highest level and temperature is at its lowest point [12].

5.2. Strategy 1

Table 6 shows the chiller performance results when the inlet gas (fuel cell exhaust gas) is blended with different ambient air quantities. The model assumes some heat losses along the duct which connects both systems. The mixing air temperature is fixed at 25 °C. In this case,

$$\dot{m}_{in} = \dot{m}_{EXTRA\,AIR} + \dot{m}_{FC\,EXH}$$

As seen in Table 6, when air is introduced at 25 °C, the mixed gas temperature drops abruptly and so does the specific heat. Therefore, although the total mass flow rate (m_{IN}) increases, the heat input (Q_{IN}) decreases due to the cooling effect. As a result, the cooling produced and COP drop. Fig. 8 shows the chiller COP versus the quantity of ambient air mixed. As seen, COP increases until it reaches a peak at 0.1 kg s^{-1} At this point, the model has not realized the temperature dropping yet, and it briefly increases the performance. However, when the temperature and specific heat drop, the COP falls rapidly.

5.3. Strategy 2

In this case, the resulting inlet temperature (T_{in}) and specific heat (C_p) also decrease as the inlet flow increase. However, they decrease less than in Strategy 1. As a result, the input heat increases, improving the chiller performance. Table 7 shows the effect of mixing a fraction of the chiller exhaust gas whereas Table 8 shows the performance results. The parameter ω represents the fraction of the total chiller exhaust gas which is being recirculated back to the chiller inlet and mixed with the fuel cell exhaust gas. It is important to note that only 40% of the mass flow rate can be recirculated. If more than 40% is recirculated, the system presents no mass conservation. As in Strategy 1, the maximum mass flow rate inlet value is

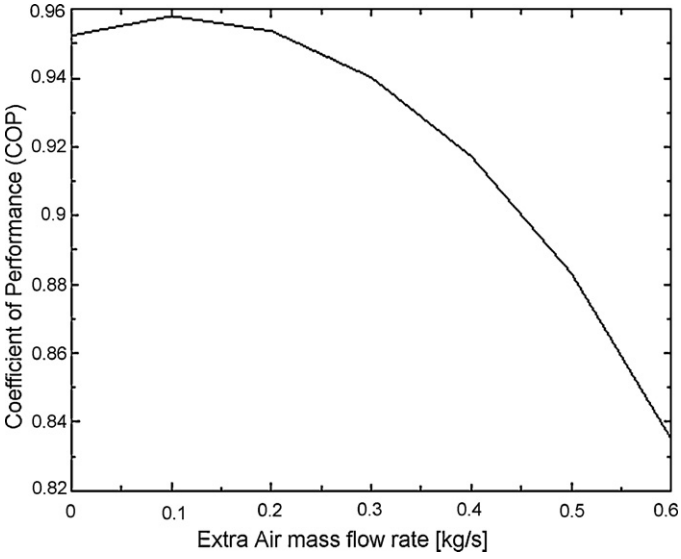

Fig. 8. Chiller COP versus extra air mass flow rate.

Table 7
Strategy 2: chiller inlet gas parameters.

w (%)	m_{FC_EXH} [kg s^{-1}]	m_{air_recvd} [kg s^{-1}]	m_{IN} [kg s^{-1}]	m_{OUT} [kg s^{-1}]	Cp_{IN} [kJ (kg K)$^{-1}$]
0	0.5099	0	0.5099	0.5099	1.264
10	0.5099	0.05666	0.5666	0.5099	1.19
20	0.5099	0.1275	0.6374	0.5099	1.115
30	0.5099	0.2185	0.7285	0.5099	1.041
35	0.5099	0.2746	0.7845	0.5099	1.004
40	0.5099	0.34	0.8499	0.5099	0.9677

Table 8
Strategy 2: performance results.

w (%)	T_{FC_EXH} [C]	T_{IN} [C]	T_{OUT} [C]	Q_{in} [kW]	Q_{CH} [kW]	COP
0	336.3	336.3	137.2	128.4	131.1	1.005
10	336.3	319.5	137.3	129.2	133.4	1.017
20	336.3	302	137.5	129.9	135.5	1.027
30	336.3	283.9	137.6	130.7	137.5	1.036
35	336.3	274.6	137.7	131.1	138.3	1.040
40	336.3	265.2	137.8	131.5	139.1	1.042
42	336.3	263.3	138	133.6	141.6	1.044

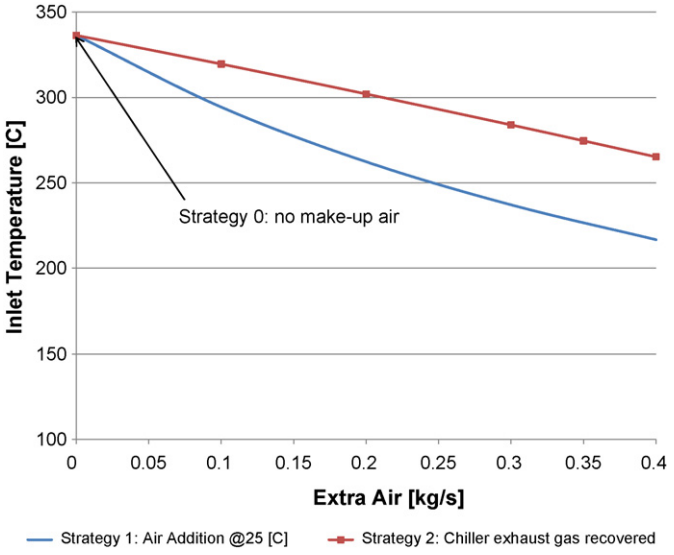

Fig. 9. Inlet temperature versus inlet air mass flow rate.

set to 0.85 kg s^{-1}. In this case,

$\dot{m}_{in} = \dot{m}_{AIR\,RECVD} + \dot{m}_{FC\,EXH}$

And $\dot{m}_{out}$ is the mass flow rate after the recirculation valve.

5.4. Strategies comparison

Figs. 9 and 10 compare the evolution of the mixed gas temperature and specific heat between Strategy 1 and Strategy 2, respectively. As seen, the inlet temperature in Strategy 1 drops more abruptly than in Strategy 2.

The same effect can be observed in Fig. 10. The gas specific heat drops more abruptly in Strategy 1 than in Strategy 2. Although inlet temperature and specific heat decrease considerably in both cases, the overall performance improves significantly with Strategy 2 as seen in Figs. 11 and 12. It is important to note that these graphs also show the chiller behavior when no extra air is injected (i.e., Strategy 0), corresponding to the point where 'Extra Air' is 0. It can be seen that the COP at this point is about 1.005 and the cooling produced is around 131.1 kW. These values are lower than the nominal values which correspond to a COP = 1.06 and Q_{CH} = 141 kW [6].

Finally, Table 9 compares the optimal operating points of the three different strategies with the nominal point provided by the manufacturer. Strategy 0 and Strategy 2 achieve similar results to the nominal point whereas Strategy 1 performance drops considerably.

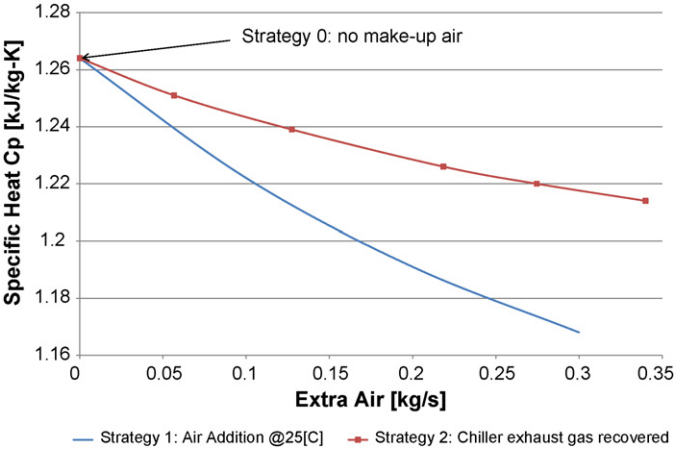

Fig. 10. Inlet gas specific heat versus extra air mass flow rate.

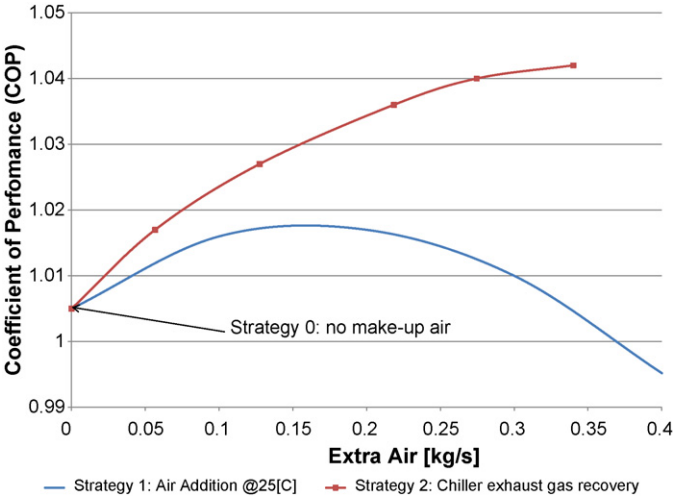

Fig. 11. COP versus extra air mass flow rate.

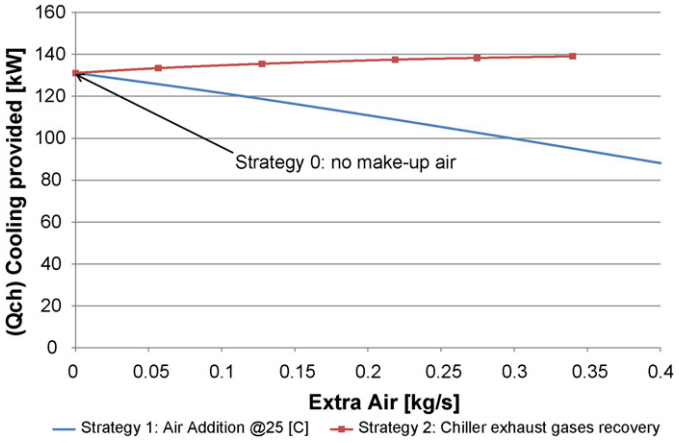

Fig. 12. Cooling provided versus extra air mass flow rate.

Table 9
Comparative Results.

	Strategy 0 m_{IN} = 0.50 [kg s^{-1}]	Strategy 1 m_{IN} = 0.85 [kg s^{-1}]	Strategy 2 m_{IN} = 0.85 [kg s^{-1}]	Nominal point
COP	1.005	0.9952	1.04	1.06
Q_{CH} [kW]	131.1	88.1	139.1	141

6. Conclusions

A 300 kW molten carbonate fuel cell and a 40 refrigeration ton direct exhaust double-effect absorption chiller have been modeled and coupled into a DG-CCHP system. The goal was to determine the readiness, applicability, utility, and suitability of commercially available fuel cell and absorption chiller products as an early DG-CCHP market entry using, as an example, a generic but realistic commercial building.

To account for the absence of a perfect match between the two units, three different coupling strategies were investigated. As a result of the simulation analyses, the following conclusions can be drawn:

- A commercially available absorption chiller, developed and designed for coupling to heat engines, can be combined with a high-temperature fuel cell to provide a viable DG-CCHP system.
- According to the chiller manufacturer, the fuel cell exhaust temperatures may be too high to be directly used in the chiller. Simulated as a baseline strategy (Strategy 0), results show acceptable performance with no risk of crystallization. Nevertheless, the manufacturer advice should be respected with the consideration of alternative strategies.
- For example, if ambient air is mixed with fuel cell exhaust gases (Strategy 1), the mass flow rate increases to the desired levels and the gas temperature is reduced. However, the reduction is gas temperature is relatively large and the chiller performance decreases compared with the nominal case.
- As an alternative, a portion of the chiller exhaust gases can be mixed with the fuel cell exhaust gases (Strategy 2). In this case, the mass flow rate increases whereas temperature does not decrease as abruptly as in Strategy 1. The result is an increase in chiller performance that exceeds the baseline strategy.

Acknowledgements

We gratefully acknowledge the Girona Fellowship and Advanced Power and Energy Program of the University of California, Irvine, which provided the financial support for this project.

We acknowledge and express deep appreciation to Tony Leo of FuelCell Energy Inc. and Masahiro Ishimatsu of Yazaki Energy Systems Inc. for their technical support and data provision used for modeling validation. In addition, we would like to thank Mr. Antoni Julia from Gas Natural (Barcelona Spain) for sharing knowledge and experience with similar systems.

References

[1] M. Medrano, J. Brouwer, V. McDonell, J. Mauzey, S. Samuelsen, Energy and Buildings 40 (2008) 537–548.
[2] DFC300MA Standard Power Plant Specification Summary, FuelCell Energy, Inc., August 2006.
[3] J. Larminie, A. Dicks, Fuel Cells Systems Explained, Second edition, Wiley, 2003.
[4] J. Brouwer, F. Jabbari, E. Martins Leal, T. Orr, Journal of Power Sources 158 (1) (2005).
[5] K. Herold, R. Radermacher, S. Klein, Absorption Chillers and Heat Pumps, CRC Press, Boca Raton, FL, 1996.
[6] Yazaki Energy, Dual Fired Chiller-Heater KE Model. 1 Specifications, 2003.
[7] G. Vliet, M. Lawson, Lithgow, Water-lithium Bromide Double Effect Absorption Cooling Analysis, Center for Energy Studies of the University of Texas at Austin, 1980.
[8] Y.A. Cengel, M.A. Boles, Thermodynamics: An Engineering Approach, sixth edition, McGraw Hill Higher Education, 2006.
[9] P. Incropera, D.P. DeWitt, Fundamentals of Heat and Mass Transfer, fifth edition, John Wiley & Sons, 2001.
[10] X. Liao, The development of an air-cooled absorption chiller concept and its integration in CHP systems. Doctor of Philosophy Dissertation. Graduate School of the University of Maryland, 2004.
[11] V. Ganaphaty, ABCO Industries, Hydrocarbon Processing (January) (1989).
[12] R.R. Pierce, Chemical Engineering (April 11) (1977).